IEEE Open Journal of
Antennas and Propagation

Received 20 March 2020; revised 10 April 2020; accepted 11 April 2020. Date of publication 15 April 2020; date of current version 7 May 2020.

Digital Object Identifier 10.1109/OJAP.2020.2988133

Bio-Matched Antennas With Flare Extensions for Reduced Low Frequency Cutoff

JOHN BLAUERT (Student Member, IEEE), AND ASIMINA KIOURTI (Senior Member, IEEE)

ElectroScience Laboratory, Department of Electrical and Computer Engineering, Ohio State University, Columbus, OH 43212, USA

CORRESPONDING AUTHOR: J. BLAUERT (e-mail: blauert.1@osu.edu)

This work was supported in part by the Consortium on Electromagnetics and Radio Frequencies.

ABSTRACT We recently reported a new class of broadband and high gain antennas for into-body radiation, called Bio-Matched Antennas (BMAs). A major limitation of our prior work is that BMA volume increases significantly as the low cutoff frequency is reduced. This is particularly troublesome for into-body applications where low operating frequencies are needed to penetrate deep into the tissues. Here, we overcome this challenge via a novel design that extends the BMA's conducting flares along the tissue surface. In doing so, the antenna's lowest operating frequency is reduced, while its volume remains unaltered. For an example BMA of 1161.3 mm^3 in volume, our new approach results in lowering the cutoff frequency from 1.9 GHz to 830 MHz. Additional novelties brought forward include: (a) the first testing of BMAs through stratified tissue models (as opposed to homogeneous models explored in the past), and (b) the smallest volume BMA reported to date, which also exhibits the lowest frequency cutoff as well as comparable or better transmission loss vs. previous designs.

INDEX TERMS Biomedical telemetry, engineered dielectrics, into-body antenna, wearable antenna.

I. INTRODUCTION

THE ADVANCEMENT of applied electromagnetics has begun to considerably impact healthcare. For example, implanted medical devices (brain implants, glucose monitors, pacemakers, etc.) can be made more ubiquitous via the use of radio frequency (RF) technology that enables wireless telemetric and charging links. In turn, these allow for around the clock monitoring of patient vitals [1]–[2], longer term implantation [3]–[4], and enhanced patient safety and comfort. As another example, medical radars can be used to image the body, allowing for non-ionizing cancer screenings [5]–[6], among other applications [7]–[8]. In other cases, high doses of RF energy can be delivered to the body to ablate malignant tissue [9]–[11]. The inverse of this, medical radiometry, has the potential to allow for non-invasive deep-tissue temperature sensing [12]–[14], as well as to passively detect tumors [15].

A major obstacle to the full integration of these technologies is the development of robust antennas capable of reliably transmitting RF waves into the body. There are numerous challenges to address in such a design: (a) mismatch at the biological tissue and antenna interface, (b) environmental and inter-subject variability, (c) frequency-dependent dielectric properties of biological tissues, and (d) inherent material loss of tissues [16].

Our previous work introduced a novel bio-matched dielectric, composed of water and plastic, to match to the biological tissues over a broad bandwidth [16], [17]. A quasi-conical antenna was constructed around this bio-matched dielectric. To improve the antenna gain, our bio-matched dielectric was further engineered to be anisotropic and keep the electric fields more normal to the direction of propagation. The end result was the Bio-Matched Antenna (BMA) [17]: a broadband, high gain antenna, capable of transmitting into the body with 15 dB less transmission loss than the state of the art [18]. A thorough discussion of the theoretical framework of the BMA is presented in [17].

However, a major limitation of BMAs is that their volume increases significantly as the low cutoff frequency is reduced. For example, reducing the low frequency cutoff from 1.4 GHz [16] to 1.1 GHz [17] results in 45% increase of the BMA volume. This is particularly troublesome for into-body applications where low operating frequencies are needed to penetrate deep into biological tissues. Concurrently, lower frequencies allow for less loss due

TABLE 1. Comparison of proposed BMAs vs. previous BMAs at 2.4 GHz.

Ref.	Phantom	BMA Volume	BMA Height	BMA Footprint	Transmission Loss	Low Frequency Cutoff	High Frequency Cutoff
[16]	80% Lean Beef (3 cm)	1773.3 mm^3	10 mm	484 mm^2	27.6 dB	1.4 GHz	8.5 GHz
[17]	80% Lean Beef (3 cm)	2572.9 mm^3	11.95 mm	620.01 mm^2	21.4 dB	1.1 GHz	11.9 GHz
This Work	Pork Belly (2.5 cm)	1161.3 mm^3	9.5 mm	364.81 mm^2	22.4 dB	1.9 GHz	9.5 GHz*
This Work	Pork Belly (2.5 cm)	1161.3 mm^3	9.5 mm	946.81 mm^2	25.1 dB	830 MHz	9.5 GHz*

*Simulated high frequency cutoffs are reported at these points, because the loss may have caused the reflection coefficient to remain below -10 dB.

FIGURE 1. BMA with a conducting flare extension to improve the low frequency cutoff.

to beam spreading, while biological tissues have less material loss at lower microwave frequencies [19].

In this paper, we take a major step forward and present a novel approach to overcoming this limitation. By extending the BMA conducting flares along the body as shown in Fig. 1, we can lower the BMA's minimum operating frequency while keeping its overall volume the same (since the conducting flares have a negligible thickness). Referring to Table 1, for an example BMA of 1161.3 mm^3 in volume, our new approach results in lowering the cutoff frequency from 1.9 GHz to 830 MHz. Such an improvement is highly valuable to the wearable antenna community, in which minimizing form factor is a high priority. Additional novelties brought forward in this work include: (a) the first testing of BMAs through stratified tissue models used to emulate the human body structure (as opposed to homogeneous materials explored in the past [16], [17]), and (b) the smallest volume BMA reported to date, which also exhibits the lowest frequency cutoff as well as comparable or better transmission loss vs. previous designs (e.g., Table 1 compares transmission loss results at 2.4 GHz). As indicated in Table 1, the only tradeoff of our new approach appears to relate to the BMA's high frequency performance; however, this is not of relevance as high frequencies are unsuitable for into-body radiation.

II. OPERATING PRINCIPLE

As shown in Fig. 1, our proposed approach relies on extending the BMA conducting flares along the body. The idea is

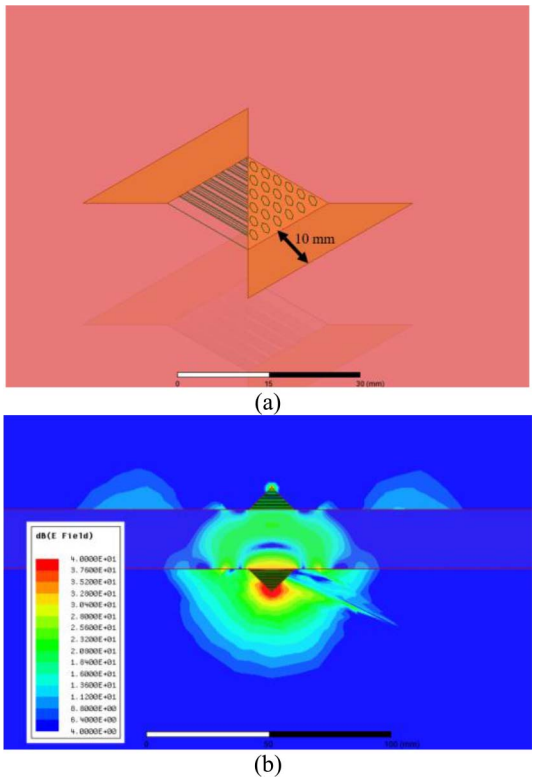

FIGURE 2. (a) Simulation setup for a BMA with a 9.5 mm height and 10 mm flare extension, and (b) electric fields for said BMA against 2.5 cm of muscle at 900 MHz.

that a more gradual wave departure can now be achieved for the antenna to improve its radiation performance [20]–[23], while the length of the current flow is increased to lower the minimal operating frequency. Concurrently, the overall antenna volume remains the same (since the conducting flares have a negligible thickness).

For example, Fig. 2 shows a Finite Element simulation carried out in Ansys HFSS for the BMA in row 4 of Table 1 placed against human muscle. As shown in Fig. 2(a), a 10 mm flare extension is added on each side of the BMA (per discussion in Section IV-A), which helps to lower the minimum frequency from 1.8 GHz to 810 MHz. Electric field simulations at 900 MHz are shown in Fig. 2(b). Here, a 2.5-cm-thick block of muscle is considered and two BMAs are placed across its two sides (to serve as transmitter and

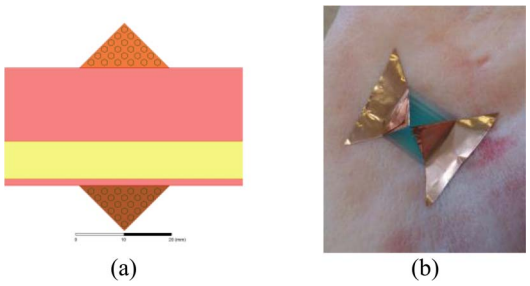

FIGURE 3. Setups employed in this study: (a) simulation setup, and (b) experimental setup.

receiver, respectively). As seen, the flares allow for a smooth transition of the fields from the antenna into the tissue, while taking up insignificant volume given their negligible thickness.

III. SIMULATION AND MEASUREMENT SETUPS

While propagation through muscle or any other homogeneous material allows for an estimate of performance, it is of the utmost importance to study propagation through stratified tissue models, which are more similar to the human body. While a variety of setups can be used, we have chosen to replicate a skin-fat-muscle model through the use of pork belly. Pork belly contains multiple stratified layers of tissue, including skin, fat and muscle. The employed simulation setup is shown in Fig. 3(a) and relies on Finite Element simulations in Ansys HFSS. Our experimental setup is shown in Fig. 3(b).

To assess the differences between human and porcine tissues, the permittivity (ε_r) and loss tangent ($\tan(\delta)$) of the pork belly are measured on both the skin side and the muscle side using Keysight's high-temperature probe [24]. Measurement result are presented in Fig. 4(a) and (b), respectively, and are found to be in good agreement. Since the pork belly has multiple layers, the dielectric probe will report different dielectric properties depending on the underlying tissues. Therefore, the exact properties of each tissue layer cannot be reported. The pig fat for instance is always in between the layers and is difficult to measure directly without destroying the phantom. In simulations, the dielectric properties corresponding to human tissues are used, as they are known to be similar to the porcine model [25] (and further verified via the super-imposed dotted lines in Fig. 4 [19]). Thickness of the tissue layers relies on average measured thicknesses of the acquired pork belly, i.e., 1.5 mm for skin, 8 mm for fat and 15.5 mm for muscle. Given that these thicknesses vary with position, they are parametrically studied in Section IV-B. It is noted that previous studies of the BMA only addressed propagation through a single medium [16]–[17]. Here, it is the first time that BMA performance is evaluated upon multiple layers of biological materials.

As a proof of concept, the BMA considered in this study has a height of 9.5 mm and a flare ascent angle of 45°, resulting in a base footprint of 19.1 × 19.1 mm^2, as shown

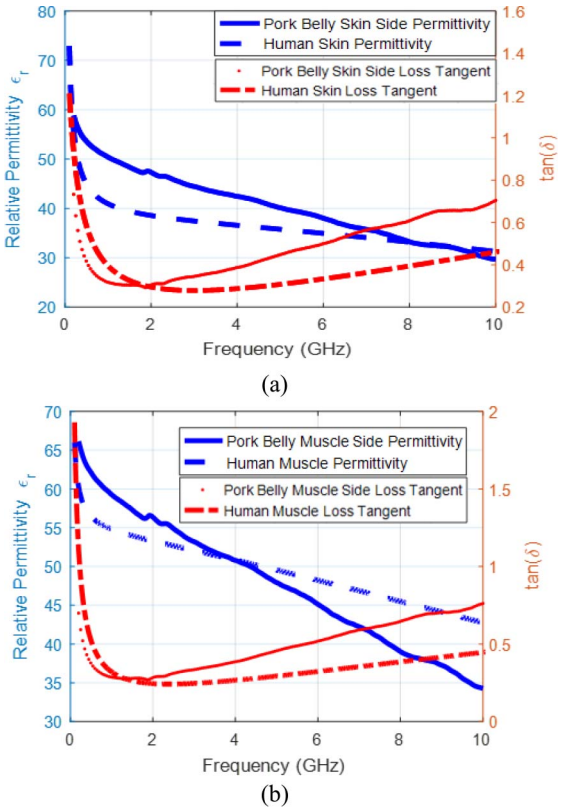

FIGURE 4. Permittivity and loss tangent measurements of (a) the pig skin side of the pork belly, and (b) the pig muscle side of the pork belly.

in Fig. 3(b). These dimensions are chosen so as to achieve a smaller volume than all previous BMAs (see Table 1), allowing the flare extensions achieve the maximum impact on the bandwidth without solely relying on antenna size. The BMA is constructed through 3D printing a dielectric base with hexagonal holes in it to hold water. The Form 2 was used as a printer for its high precision for small features [26]. To improve water retention, a two percent (2%) gelatin type A hydrogel is employed. Its electrical properties are very similar to water as measured via Keysight's high-temperature probe, Fig. 5(a). To observe potential water leakage, the hydrogel was dyed blue and the clear resin was used for 3D printing. The clear resin's electrical properties are also measured, as shown in Fig. 5(b).

IV. SIMULATION RESULTS

A. FLARE EXTENSION PARAMETRIC STUDIES

Using the average material thicknesses presented in Section III, the BMA is simulated with 45° flare extensions. To understand the tradeoffs of flare extensions, the length of the flare extensions applied to the BMA is parametrically swept in simulation from 0 to 15 mm in 5 mm increments. The reflection coefficients from these sweeps are shown in Fig. 6(a). With an extension of 10 mm on each side, the BMA can cover the 886-906 MHz Industrial, Scientific, and Medical (ISM) applications band [27] without increasing antenna volume. Indeed, Fig. 6(a) shows that

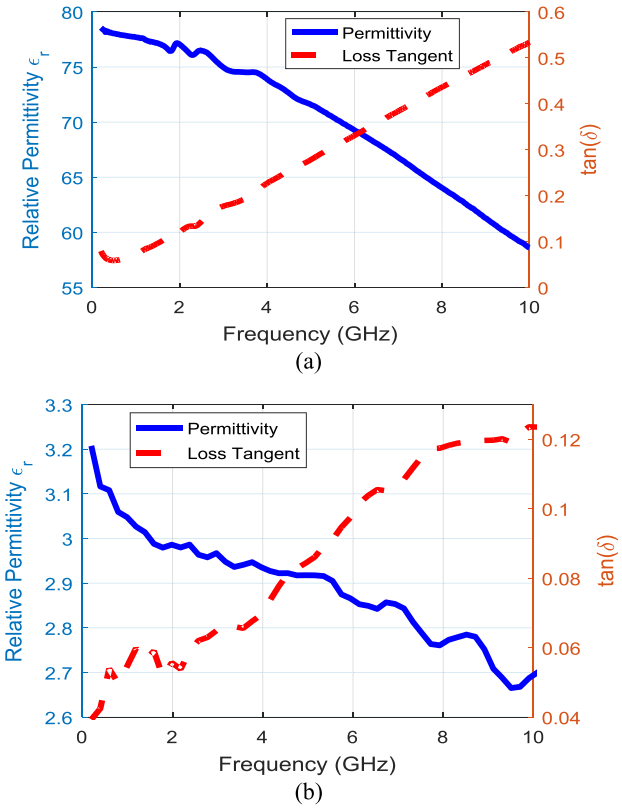

FIGURE 5. Permittivity (ε_r) and loss tangent (tanδ) measurements of the: (a) hydrogel and (b) clear resin used to fabricate the BMA.

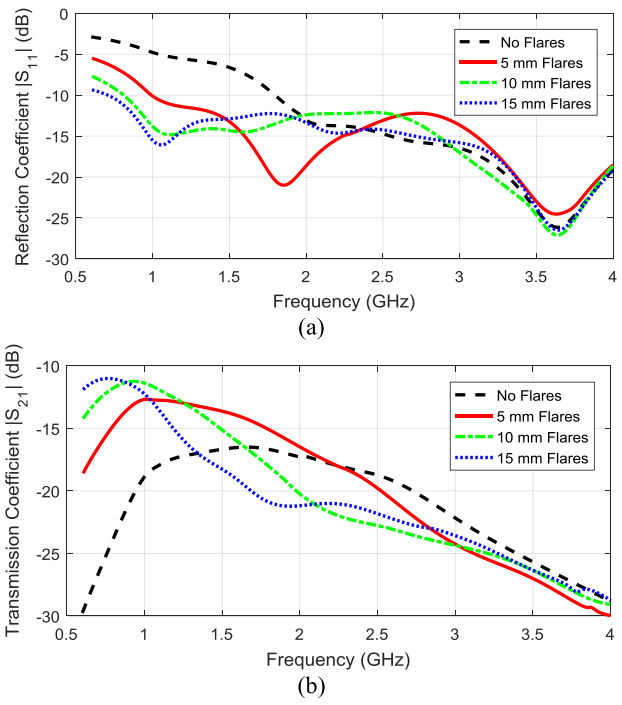

FIGURE 6. BMAs with varying flare extensions (a) reflection coefficient and (b) transmission coefficient.

a flare extension of 10 mm to the original design (without the flares) lowers the cutoff frequency from 1.8 GHz to 810 MHz.

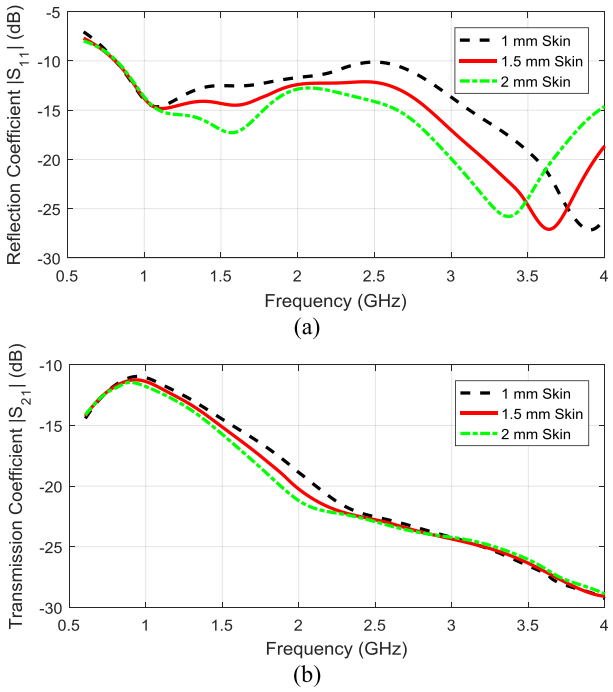

FIGURE 7. BMAs with varying skin thickness (a) reflection coefficient and (b) transmission coefficient.

Additionally, the transmission coefficient through 2.5 cm of stratified tissue layers is reported in Fig. 6(b). At higher frequencies, BMAs with smaller flares outperform BMAs with larger flares. This most likely stems from the smaller flare extensions improving their gain when propagating through the anisotropic bio-matched dielectric. However, as the frequency becomes higher (∼3.5 GHz), the transmission and reflection coefficient become comparable. This is because the BMA no longer primarily relies on the flares for propagation.

B. PARAMETRIC STUDIES ON TISSUE THICKNESS

Using the 10 mm flare extensions on the BMA, the tissue thicknesses are varied in simulation to assess their impact on antenna performance. The total thickness of the skin, fat and muscle layers is kept to 2.5 cm in order to assess transmission more directly. In the initial case, the fat thickness is kept at 8 mm while the skin thickness is varied from 1 to 2 mm. There are marginal impacts in reflection and transmission coefficients as shown in Fig. 7(a) and 7(b), respectively.

Next, the skin layer is kept at a 1.5 mm thickness and the fat thickness is varied from 6 to 10 mm. There is once again a limited impact in the reflection and transmission coefficient, as reported in Fig. 8(a) and 8(b), respectively.

V. MEASUREMENT RESULTS

The BMA from Section IV is constructed with a 10 mm flare extension and placed on top of the pork belly as shown in Fig. 3(b). The measured and simulated reflection coefficient are shown in Fig. 9(a). As seen, there is good agreement

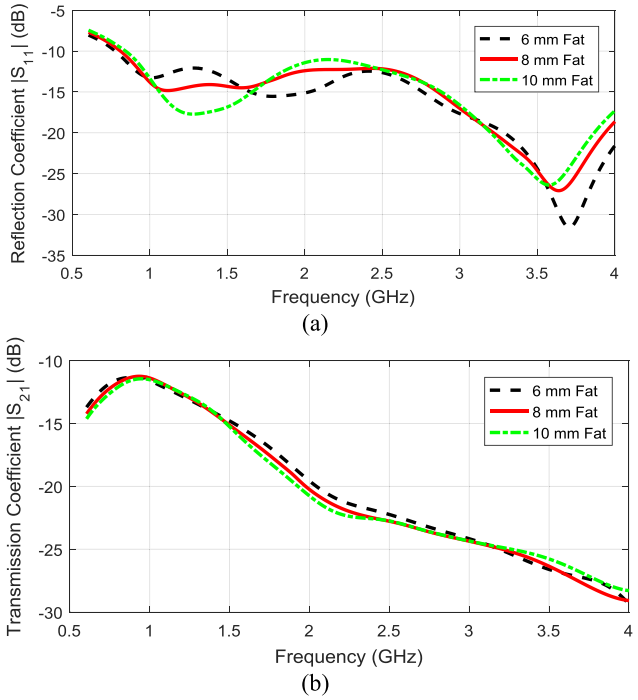

FIGURE 8. BMAs with varying fat thickness (a) reflection coefficient and (b) transmission coefficient.

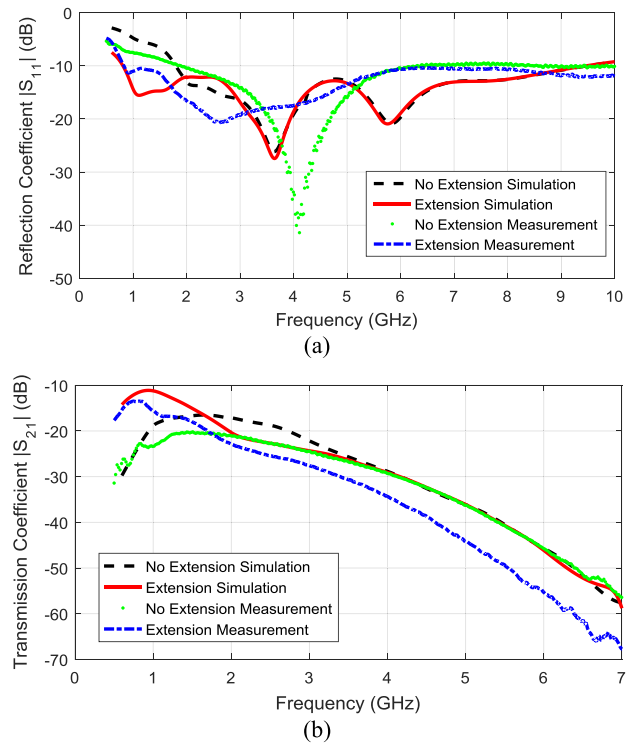

FIGURE 9. Measurement and simulation results for the (a) reflection coefficient and (b) transmission coefficient.

between the designs and the 11.4:1 bandwidth extends from 830 MHz to ∼9.5 GHz.

Additionally, the transmission coefficient is measured and reported in Fig. 9(b). The transmission loss through 2.5 cm of tissue is a remarkable 14.0 dB in the ISM band at 900 MHz [27]. Transmission degrades exponentially with frequency, and the BMA performance is limited at higher frequencies. However, this is not of relevance as high frequencies are unsuitable for into-body radiation. Another observation is that the measurements do not show comparable transmission between the extended flare BMA and the original BMA at higher frequencies. The discrepancies at higher frequencies is most likely due to the flares not being perfectly uniform across the surface and having wrinkles in them, since they were constructed with copper tape. This would be more impactful at higher frequencies than lower frequencies. Additionally, there could have been positional and rotational misalignment of the BMA along the pork belly.

VI. SPECIFIC ABSORPTION RATE (SAR) PERFORMANCE

With such a high amount of copper making direct contact with the biological tissues, one must consider the specific absorption rate (SAR) implications of flare extensions upon the BMA. When contrasting maximum power input to comply with the Federal Communications Commission (FCC) limit of 1.6 W/kg for SAR_{1g} [28] at 2 GHz, we report that BMAs with a 10 mm flare extension can use 11.8 mW of maximum input power. By contrast, BMAs with no extensions can use 18.8 mW of maximum input power. However, both types of BMA have comparable maximum input power when used at frequencies greater than 2.5 GHz. This is because the BMAs with flare extensions no longer heavily rely upon the flare extensions for propagation at those frequencies.

VII. CONCLUSION

The intersection of electromagnetics and medical devices can be made more impactful through high gain and broadband into-body antennas. The work in this paper demonstrates that BMAs maintain these desirable characteristics when propagating into stratified media as well as previously reported homogeneous media. Additionally, we have demonstrated that the minimum operating frequency can be lowered without increasing antenna volume through the extension of the conducting flares. This allows for a very low transmission loss of 14.0 dB through 2.5 cm of biological tissues at 900 MHz, using the smallest volume BMA reported to date. A tradeoff is introduced through the extended BMAs having lower transmission loss at middle frequencies, but both types of antenna have comparable transmission at higher frequencies.

REFERENCES

[1] J. Kim and Y. Rahmat-Samii, "Implanted antennas inside a human body: Simulations, designs, and characterizations," *IEEE Trans. Microw. Theory Techn.*, vol. 52, no. 8, pp. 1934–1943, Aug. 2004.

[2] C. C. Y. Poon, B. P. L. Lo, M. R. Yuce, A. Alomainy, and Y. Hao, "Body sensor networks: In the era of big data and beyond," *IEEE Rev. Biomed. Eng.*, vol. 8, pp. 4–16, Apr. 2015.

[3] P. Anacleto, P. M. Mendes, E. Gultepe, and D. H. Gracias, "3D small antenna for energy harvesting applications on implantable micro-devices," in *Proc. Loughborough Antennas Propag. Conf.*, Loughborough, U.K., Nov. 2012, pp. 1–4.
[4] B. J. DeLong, A. Kiourti, and J. L. Volakis, "A radiating near-field patch rectenna for wireless power transfer to medical implants at 2.4 GHz," *IEEE J. Electromagn. RF Microw. Med. Biol.*, vol. 2, no. 1, pp. 64–69, Mar. 2018.
[5] M. Klemm, J. A. Leendertz, D. Gibbins, I. J. Craddock, A. Preece, and R. Benjamin, "Microwave radar-based breast cancer detection: Imaging in inhomogeneous breast phantoms," *IEEE Antennas Wireless Propag. Lett.*, vol. 8, pp. 1349–1352, Nov. 2009.
[6] A. E. Fouda and F. L. Teixeira, "Ultra-wideband microwave imaging of breast cancer tumors via Bayesian inverse scattering," *J. Appl. Phys.*, vol. 115, no. 6, Feb. 2014, Art. no. 064701.
[7] E. Schires, P. Georgiou, and T. S. Lande, "Vital sign monitoring through the back using an UWB impulse radar with body coupled antennas," *IEEE Trans. Biomed. Circuits Syst.*, vol. 12, no. 2, pp. 292–302, Apr. 2018.
[8] F. Wang, Y. Chou, Y. Chiu, and T. Horng, "Chest-worn health monitor based on a bistatic self-injection-locked radar," *IEEE Trans. Biomed. Eng.*, vol. 62, no. 12, pp. 2931–2940, Dec. 2015.
[9] C. H. N. Reimann *et al.*, "A dual-mode coaxial slot applicator for microwave ablation treatment," *IEEE Trans. Microw. Theory Techn.*, vol. 67, no. 3, pp. 1255–1264, Mar. 2019.
[10] H. Luyen, F. Gao, S. C. Hagness, and N. Behdad, "Microwave ablation at 10.0 GHz achieves comparable ablation zones to 1.9 GHz in ex vivo bovine liver," *IEEE Trans. Biomed. Eng.*, vol. 61, no. 6, pp. 1702–1710, Jun. 2014.
[11] J. Chiang, S. Birla, M. Bedoya, D. Jones, J. Subbiah, and C. L. Brace, "Modeling and validation of microwave ablations with internal vaporization," *IEEE Trans. Biomed. Eng.*, vol. 62, no. 2, pp. 657–663, Feb. 2015.
[12] D. Rodrigues *et al.*, "Design and optimization of an ultra wideband and compact microwave antenna for radiometric monitoring of brain temperature," *IEEE Trans. Biomed. Eng.*, vol. 61 no. 7, pp. 2154–2160, Jul. 2014.
[13] N. Livanos *et al.*, "Design and interdisciplinary simulations of a hand-held device for internal-body temperature sensing using microwave radiometry," *IEEE Sens. J.*, vol. 18, no. 6, pp. 2421–2433, Mar. 2018.
[14] P. Momenroodaki, W. Haines, M. Fromandi, and Z. Popovic, "Noninvasive internal body temperature tracking with near-field microwave radiometry," *IEEE Trans. Microw. Theory Techn.*, vol. 66, no. 5, pp. 2535–2545, May 2018.
[15] T. Sugiura, H. Hirata, J. W. Hand, J. M. J. Van Leeuwen, and S. Mizushina, "Five-band microwave radiometer system for noninvasive brain temperature measurement in newborn babies: Phantom experiment and confidence interval," *Radio Sci.*, vol. 46, no. 5, pp. 1–7, Oct. 2011.
[16] J. Blauert and A. Kiourti, "Bio-matched horn: A novel 1–9 GHz on-body antenna for low-loss biomedical telemetry with implants," *IEEE Trans. Antennas Propag.*, vol. 67, no. 8, pp. 5054–5062, Aug. 2019.
[17] J. Blauert and A. Kiourti, "Theoretical modeling and design guidelines for a new class of wearable bio-matched antennas," *IEEE Trans. Antennas Propag.*, vol. 68, no. 3, pp. 2040–2049, Mar. 2020.
[18] J. M. Felício, J. R. Costa, and C. A. Fernandes, "Dual-band skin-adhesive repeater antenna for continuous body signals monitoring," *IEEE J. Electromagn. RF Microw. Med. Biol.*, vol. 2, no. 1, pp. 25–32, Mar. 2018.
[19] C. Gabriel, "Compilation of the dielectric properties of body tissues at RF and microwave frequencies," Brooks Air Force Base, San Antonio, TX, USA, Rep. N.AL/OE-TR- 1996-0037, Jun. 1996.
[20] K.-H. Lee, C.-C. Chen, F. L. Teixeira, and R. Lee, "Modeling and investigation of a geometrically complex UWB GPR antenna using FDTD," *IEEE Trans. Antennas Propag.*, vol. 52, no. 8, pp. 1983–1991, Aug. 2004.
[21] C. Handel, I. J. Gupta, and W. D. Burnside, "Low frequency modification of a dual chamber compact range," Dept. ElectroSci. Lab., Ohio State Univ., Columbus, OH, USA, Rep. 732 264, Sep. 1997.
[22] L. Chaung, T. Chang, and W. D. Burnside, "An ultrawide-bandwidth tapered resistive TEM horn antenna," *IEEE Trans. Antennas Propag.*, vol. 48, no. 12, pp. 1848–1857, Dec. 2000.
[23] M. S. A. Mahmoud, T.-H. Lee, and W. D. Burnside, "Enhanced compact range reflector concept using an R-card fence: Two-dimensional case," *IEEE Trans. Antennas Propag.*, vol. 49, no. 3, pp. 419–428, Mar. 2001.
[24] (2020). *N1501A Dielectric Probe Kit*. [Online]. Available: https://www.keysight.com/en/pd-2492144-pn-N1501A/dielectric-probe-kit?cc=US&lc=eng
[25] T. Karacolak, R. Cooper, E. S. Unlu, and E. Topsakal, "Dielectric properties of porcine skin tissue and in vivo testing of implantable antennas using pigs as model animals," *IEEE Antennas Wireless Propag. Lett.*, vol. 11, pp. 1686–1689, 2012.
[26] (2019). *Formlabs*. [Online]. Available: www.formlabs.com
[27] OET Bulletin, *ITU-R Radio Regulations Section 5.138 and 5.150* Int. Telecommun. Union-Radiocommun., Geneva, Switzerland, 1997.
[28] *Evaluating Compliance With FCC Guidelines for Human Exposure to Radio Frequency Electromagnetic Fields*, FCC, Washington, DC, USA, Jun. 2001.